

Drop splashing is independent of substrate wetting

Andrzej Latka* and Sidney R. Nagel

*The James Franck Institute and Department of Physics,
The University of Chicago, 929 E 57th Street, Chicago, Illinois 60637, USA*

Arnout M. P. Boelens and Juan J. de Pablo

*Institute for Molecular Engineering, The University of Chicago,
5801 South Ellis Avenue, Chicago, Illinois 60637, USA*

A liquid drop impacting a dry solid surface with sufficient kinetic energy will splash, breaking apart into numerous secondary droplets. This phenomenon shows many similarities to forced wetting, including the entrainment of air at the contact line. Because of these similarities and the fact that forced wetting has been shown to depend on the wetting properties of the surface, existing theories predict splashing to depend on wetting properties as well. However, using high-speed interference imaging we observe that wetting properties have no effect on splashing for various liquid-surface combinations. Additionally, by fully resolving the Navier-Stokes equations at length and time scales inaccessible to experiments, we find that the shape and motion of the air-liquid interface at the contact line are independent of wettability. We use these findings to evaluate existing theories and to compare splashing with forced wetting.

PACS numbers: 47.20Gv, 47.55.dr, 47.55.np.

At first glance, the same physics should describe a solid plunging into a liquid and a liquid drop impacting a solid: both scenarios revolve around a liquid-gas-solid contact line that is forced to move at large velocities. In the former case, exceeding a critical contact line velocity leads to the destabilization of the contact line and the entrainment of gas bubbles in the liquid. This phenomenon, called dewetting [1] or wetting failure [2], is also observed in drop impact [3]. It has therefore been suggested that the onset of contact line instability can serve as an onset criterion for drop splashing [4].

Models of forced wetting [1, 5] use the wetting properties of the surface as a boundary condition to determine the stability threshold for the contact line. Indeed, the wettability of the object that is plunged into or withdrawn from a liquid has been found to have a strong influence on wetting failure [6]. In contrast, we present experimental results which show that, for a wide array of liquids, the surface wettability has no effect on splashing. We also describe simulations that are able to resolve contact line behavior at high resolution. These simulations reveal that the contact line motion previously associated with splashing on completely wetting surfaces [7], is nearly identical for a completely non-wetting surface. Before dewetting, the rapidly moving contact line in both the wetting and the non-wetting case shows a microscopic contact angle of 180° . This suggests that the assumption of a fixed microscopic contact angle is inapplicable to contact lines that are forced to move at high speeds, as is the case in splashing, and challenges theories based on this assumption.

I. METHODS

A. Experiments

The experiments were conducted with either silicone oil (PDMS, Clearco Products) of viscosity $\mu = 9.4$ and 32cP or a mixture of water and glycerol ($\mu = 32$ cP). The drops with diameter $D = 3.3 \pm 0.1$ mm were produced at a nozzle with a syringe pump and were accelerated by gravity to an impact velocity of $V = 3.4 \pm 0.1$ ms⁻¹. The silicone oil drops impacted glass slides (Fisherbrand Microscope Slides) that were left untreated to provide a wetting surface, with contact angle $\theta_0 = 0^\circ$, or glass slides covered with an oleophobic coating (Fussode Coat, $\theta_0 = 42 \pm 2^\circ$). Similarly, the water-glycerol drops impacted either clean glass ($\theta_0 = 36 \pm 3^\circ$), glass coated with indium tin oxide ($\theta_0 = 79 \pm 4^\circ$) or a hydrophobic coating (RainX, $\theta_0 = 90 \pm 3^\circ$). A wetting substrate was achieved for the water-glycerol by pre-wetting the glass slide with the same mixture. A liquid drop fully wets such a prepared slide ($\theta_0 = 0^\circ$), however the coating is thin enough not to change the splashing behavior. The changing of substrates only affects the contact angle and does not change the spreading dynamics. Figure 2 shows that drops spread at the same rate regardless of θ_0 . Air was used as the ambient gas, whose pressure P was controlled in a vacuum chamber ($5\text{kPa} \leq P \leq 101\text{kPa}$). Impacts were recorded with high-speed cameras (Vision Research) at rates up to 130 000 fps either from the side as in Fig. 1(a-c), or with interference imaging (d-f). The latter method measures the interference between light reflected from the bottom surface of the spreading liquid and the top surface of the substrate. Wherever the liquid is in contact with the substrate, destructive interference results in no light entering the camera. Wherever the two are separated, an interference pattern is created, as seen

* alatka@uchicago.edu

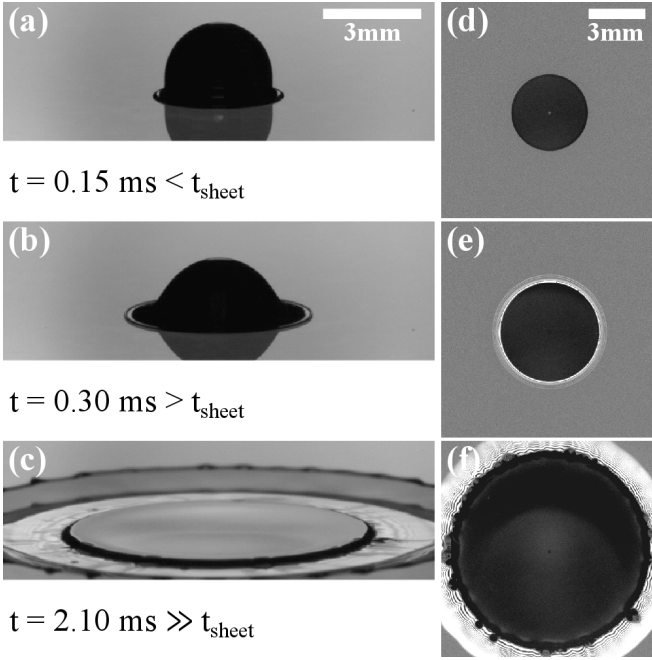


Figure 1. Successive images of a 9.4cP silicone oil drop of diameter 3.2 mm impacting a glass slide at 3.3 m/s at atmospheric pressure. Images (a) - (c) show the side view of the drop and its reflection, while (d) - (f) show the interference measurement from below at corresponding times. Initially, the drop spreads fully wetting the substrate in the form of a lamella. After time $t_{\text{sheet}} = 0.21\text{ms}$ an air gap appears between the liquid and solid, seen clearly as bright interference fringes (e,f), resulting in the creation of a thin liquid sheet (b,c) that extends from the thicker lamella.

in Fig. 1(e-f). Since this method is particularly sensitive to the presence of the air gap, it allows us to measure precisely when the contact line begins to entrain air [3].

A typical splash is presented in the left column of Fig. 1. Figure 1(a) shows that a drop does not splash immediately. Instead the liquid spreads radially outward in the form of a lamella [8, 9]. The simultaneous interference image shows that the lamella fully wets the substrate. Beginning at time t_{sheet} after impact one can observe an interference pattern at the liquid-air-solid contact line, as in Fig. 1(e), indicating the presence of a micron thick gas film separating the spreading liquid from the substrate. The time t_{sheet} is the start of the formation of a thin sheet of liquid [3, 8], as can be seen in Fig. 1(b). The thin sheet grows and ultimately breaks up into the secondary droplets that form the splash ($t = 2.1\text{ms}$, Fig. 1(c,f)).

The thin sheet creation time depends on a number of parameters [8]. Most importantly, t_{sheet} is delayed as the ambient gas pressure is reduced. However, if the pressure is decreased below a threshold pressure P_{sheet} , instead of being further delayed, the thin sheet will fail to appear and the splash will have been completely suppressed [10–12]. We quantify the effect of wetting on splashing by measuring the dependence of both t_{sheet} and P_{sheet} on

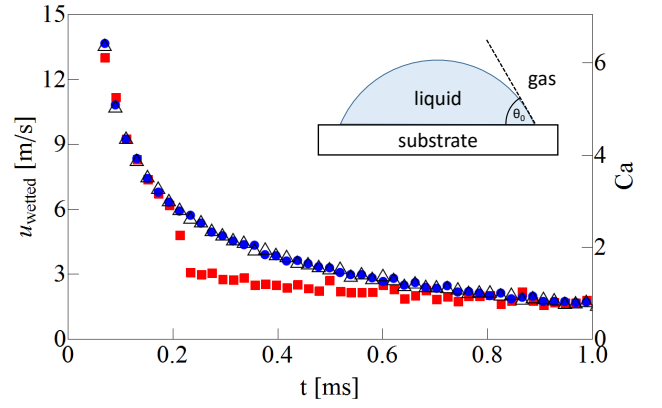


Figure 2. Speed of the advancing liquid-solid contact line as a function of time after impact of a 9.4cP silicone oil drop on glass ($\theta_0 = 0^\circ$, \blacktriangle) or glass coated with an oleophobic layer ($\theta_0 = 42^\circ$, \blacktriangle). Splashing was suppressed by reducing the pressure to $P = 30\text{kPa} < P_{\text{sheet}}$. The presence of a coating does not influence spreading speed. At atmospheric pressure (\blacksquare) air entrainment begins at $t_{\text{sheet}} = 0.21\text{ms}$ after which the contact line slows. The diagram shows that Young's angle θ_0 , at which a stationary gas-liquid interface meets the substrate, is measured in the liquid phase.

the surface properties.

B. Simulations

To be able to examine the contact line in more detail, we simulate the breakup of a splashing drop using a finite volume implementation of the volume of fluid method [13]. This method tracks the different phases in the system by using a phase parameter, α , which is 0 in the gas phase, 1 in the fluid phase, and has an intermediate value at the interface. The evolution of the phase parameter field is calculated using its own transport equation. The phase parameter field is used to find the phase averaged density, velocity, and viscosity, which are in turn used to evolve the Navier-Stokes equations. The parameter α is also used to calculate the surface tension using the Brackbill surface tension model [14].

The effect of varying the Young's angle θ_0 from 0° to 180° is calculated directly through the generalized Navier boundary condition at the impact wall [15, 16]. With this boundary condition the dynamic contact angle θ is allowed to vary freely, but a restoring line-tension force is applied at the contact line whenever the dynamic angle deviates from θ_0 . This restoring force is an additional source term in the Navier-Stokes equations, and has the following form:

$$\vec{f}_{\text{lt}} = -\frac{\sigma}{h} \cos \theta_0 \nabla_{2D} \alpha \quad (1)$$

In the above equation σ is the surface tension coefficient, h is the height of the local grid cell, and $\nabla_{2D} \alpha$

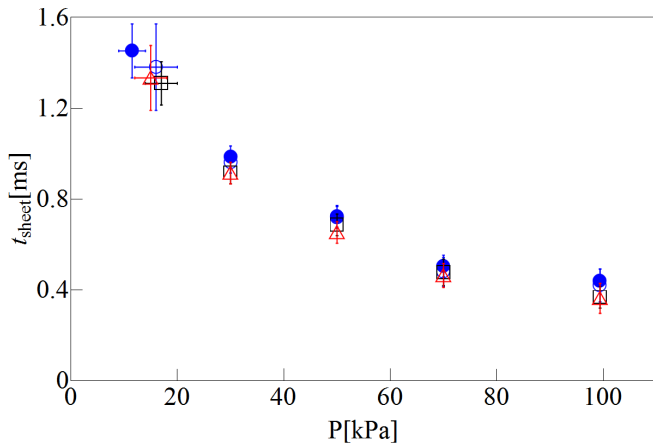


Figure 3. Time of thin sheet creation vs. ambient gas pressure for impacts of 32cP water-glycerol drops on glass slides with $\theta_0 = 0^\circ$ (●), 36° (○), 79° (□), and 90° (△). t_{sheet} is independent of wetting.

is the gradient of α on the wall. This force is applied on the liquid-gas interface in the first grid cells adjacent to the wall and is balanced by the surface tension force when θ is equal to θ_0 . The simulations are performed for ethanol in air using the VOF solver of the OpenFOAM Finite Volume toolbox [17] at up to 10nm resolution at the wall. More information on the equations, boundary conditions, initial conditions, and the validity of these methods can be found in references [7] and [18].

To reduce memory requirements, we consider an ethanol ($\mu = 1.1\text{cP}$) droplet with a diameter of $300\mu\text{m}$, as opposed to the 3mm more viscous droplets used in the experiments. As the splashing threshold has been shown to scale across a wide range of parameters [4, 19], comparisons with experiments should not be compromised.

II. RESULTS

A. Experiments

Varying the surface wettability does not affect t_{sheet} , as shown for water-glycerol drops in Fig. 3. Notably, the onset of thin sheet creation is surprisingly independent of changes in surface properties. Not only does a hydrophobic coating fail to change t_{sheet} , but even coating the glass slide with a thin layer of water-glycerol yields the same result. Similarly, no noticeable effect of wetting can be seen for silicone oil drops in Fig. 4, where the substrate was changed from fully wetting with $\theta_0 = 0^\circ$ to partially wetting with $\theta_0 = 42^\circ$.

Figure 5 compares the threshold pressure for the different substrates. As the ambient pressure is decreased, t_{sheet} is delayed and the resulting thin sheet is diminished. Consequently, below a pressure P_{splash} , the thin sheet is too small to break apart into secondary droplets and splashing is suppressed. If the ambient pressure is

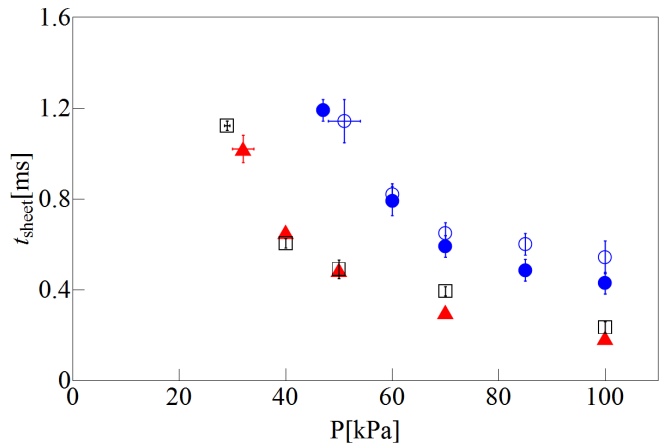


Figure 4. Time of thin sheet creation vs. ambient gas pressure for impacts of 9.4cP silicone oil drops on glass slides with $\theta_0 = 0^\circ$ (●) and 42° (○), and of 32cP silicone oil drops on glass slides with θ_0 of 0° (▲) and 42° (□). The small differences in t_{sheet} with wetting properties are within error.

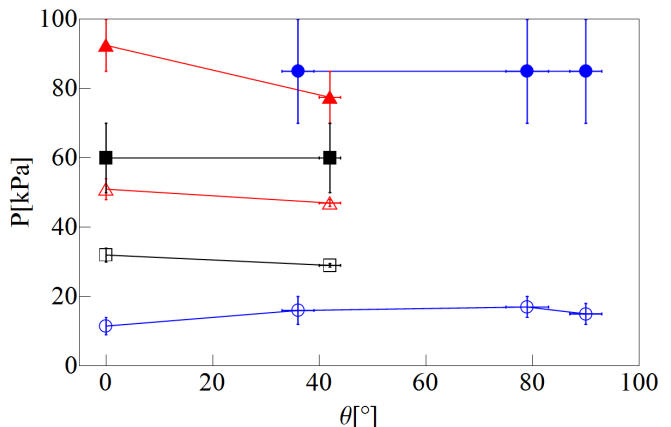


Figure 5. Threshold pressure for drop breakup P_{splash} (filled symbols) and thin sheet creation P_{sheet} (empty symbols) vs. contact angle: 32cP water-glycerol (●), 32cP silicone oil (▲) and 9.4cP silicone oil (■). Thin sheets created at $P_{\text{sheet}} < P < P_{\text{splash}}$ will not break apart. Neither threshold is affected by surface wettability.

further decreased below P_{sheet} , the thin sheet is never formed. We find that both P_{sheet} and P_{splash} are independent of θ_0 . This result is similar to the velocity threshold in Ref. [6], which was also independent of θ_0 for $\theta_0 < 90^\circ$.

B. Simulations

The simulation results shown in Fig. 6 compare the shape of the air-liquid interface for wetting and non-wetting surfaces at different stages of impact. To facilitate comparisons with experiments, velocity is non-dimensionalized as the capillary number $\text{Ca} \equiv \frac{\mu V}{\sigma}$. At all

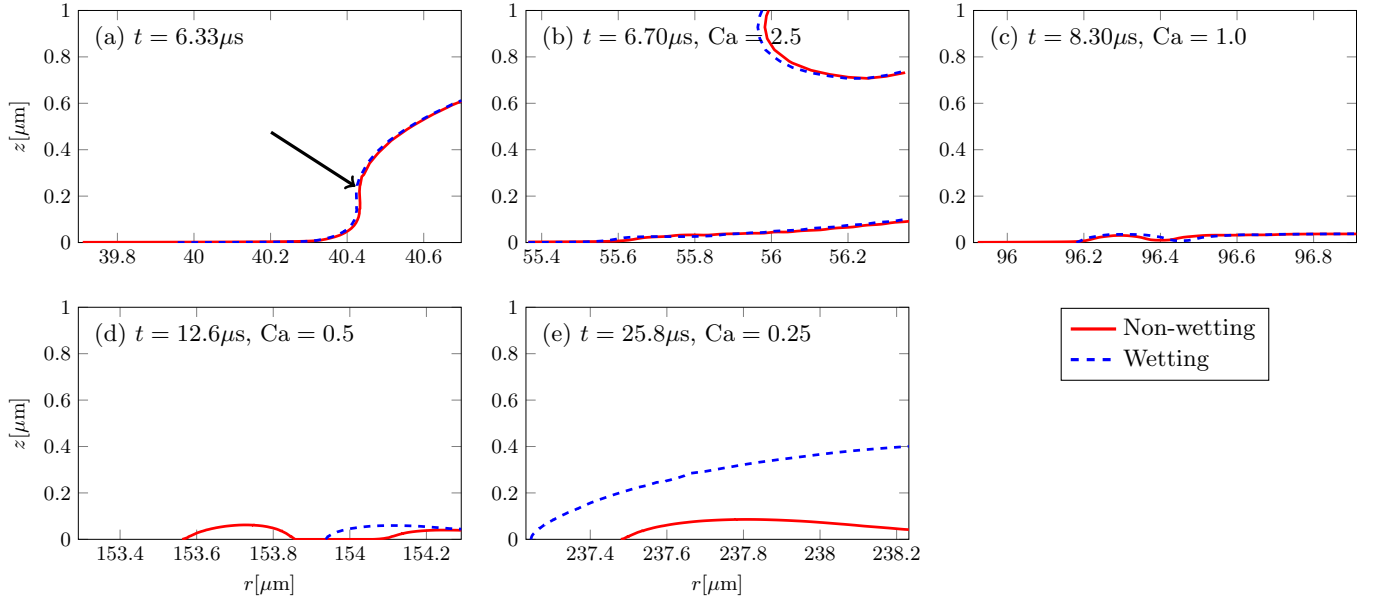


Figure 6. Time series of the droplet interface showing the contact line evolution for a simulated droplet with the parameters of ethanol at atmospheric pressure for $\theta_0 = 0^\circ$ (wetting) and $\theta_0 = 180^\circ$ (non-wetting). The vertical axis shows height above the surface and the horizontal axis shows the radial distance from the point of impact. (a) The moment a cusp (indicated by the black arrow) can first be observed in the interface. This is the onset of lamella formation. (b) Immediately after t_{sheet} . A gas film is present under the liquid sheet and the interface approaches the surface at a 180° angle. (c) The transition from the $\text{Ca} > 1$, high-speed contact line regime to the $\text{Ca} < 1$, low-speed regime. (d) As explained in section II B, this frame shows a touch-down event of the interface on the non-wetting surface: a gas bubble is entrained behind the contact line. (e) The gas film forming on the wetting surface at low speeds is thicker than the gas film on the non-wetting surface.

times for which $\text{Ca} > 1$ the interface is the same on both surfaces and, within the resolution of the simulations, the microscopic contact angle in both cases is 180° .

Only for times at which $\text{Ca} \leq 1$ do the interfaces begin to look different; the contact angle on the non-wetting surface remains 180° , while the contact angle on the wetting surface decreases and would converge to its equilibrium Young's angle, $\theta_0 = 0^\circ$, if the simulation were to run long enough until the drop is stationary.

A consequence of the lower θ in the wetting case at low Ca is a thicker gas film at the contact line compared to the non-wetting surface, as can be observed most clearly in Fig. 6 (e). Independent of the wetting properties, the gas film thickness is greatest when the air-liquid interface becomes parallel to the substrate (cf. Figs. 6 (c-e)). The lower θ at the contact line of a wetting substrate requires a longer arc length to satisfy this condition, which results in a thicker gas film. Additionally, a greater separation between the liquid sheet and the substrate stabilizes the contact line. At early times, the gas film in front of the contact line periodically collapses and the liquid touches down on the substrate, entraining air bubbles (Fig. 6 (d)). The contact line on the non-wetting surface never stabilizes and bubbles are entrained throughout the simulation. In contrast, these touch-down events are no longer observed at late times on the wetting surface.

A quantitative description of the differences in contact line behavior for splashing on wetting versus non-wetting

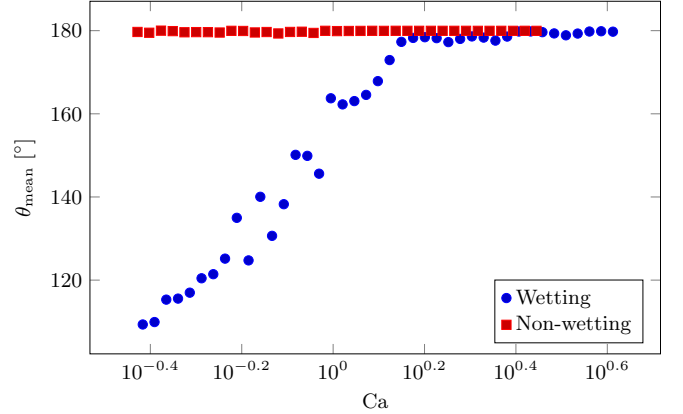


Figure 7. Average mean contact angle as a function of the capillary number for a simulated droplet with the parameters of ethanol at atmospheric pressure. For wetting surfaces a transition can be observed for $\text{Ca} \approx 1$ where the microscopic angle goes from $\theta < 180^\circ$ to $\theta = 180^\circ$. For the non-wetting surface the microscopic angle stays constant.

surfaces is provided in Fig. 7 by plotting the microscopic contact angle as function of the capillary number for wetting and non-wetting surfaces. In agreement with Fig. 6, for $\text{Ca} > 1$ both wetting and non-wetting surfaces show the same contact angle of 180° . When the contact line slows to $\text{Ca} < 1$ the non-wetting surface continues to

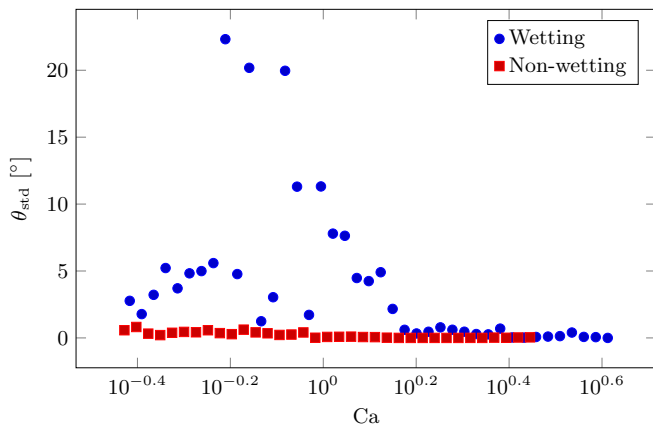


Figure 8. Standard deviation of the contact angle as a function of the capillary number for a simulated droplet with the parameters of ethanol at atmospheric pressure. For wetting surfaces, the contact line regime change around $Ca \approx 1$ causes the fluctuations of the microscopic contact angle to increase significantly. This increase in fluctuations is not observed for non-wetting surfaces.

exhibit $\theta = 180^\circ$, while the wetting surface exhibits a contact angle that decreases with Ca .

The change of behavior at $Ca \approx 1$ is shown via the standard deviation of the microscopic contact angle in Fig. 8. For the non-wetting surface $\theta = 180^\circ$ at all times, therefore the fluctuations are small and independent of the capillary number. For the wetting surface at large capillary numbers the fluctuations are also small, however shortly before $Ca = 1$ they begin to grow dramatically as $Ca \rightarrow 1$. This behavior is reminiscent of a phase transition, where fluctuations increase around the critical point. Taking this analogy further, this suggests that not only does the contact angle change for $Ca < 1$, but, more importantly, the flow enters a different flow regime. Note that this result is unrelated to the aforementioned touch-down events, which are instabilities of the apparent contact angle.

Figures 9 and 10 show the horizontal and vertical liquid sheet ejection velocities, measured at the rim of the liquid sheet. Figure 6 shows that a cusp forms in the interface at the same time for both wetting and non-wetting surfaces. Consequently, one can expect the liquid sheet, which forms promptly after the cusp can be detected, to be ejected at the same velocity. This is confirmed in Figs. 9 and 10, which demonstrate that the liquid sheets are ejected at the same angle, independent of wetting properties. As time progresses the figures show that the trajectories of the liquid sheet are nearly identical for the wetting and non-wetting case.

III. DISCUSSION

The key to understanding the unusual contact line behavior in splashing is in contrasting it with that of slow-

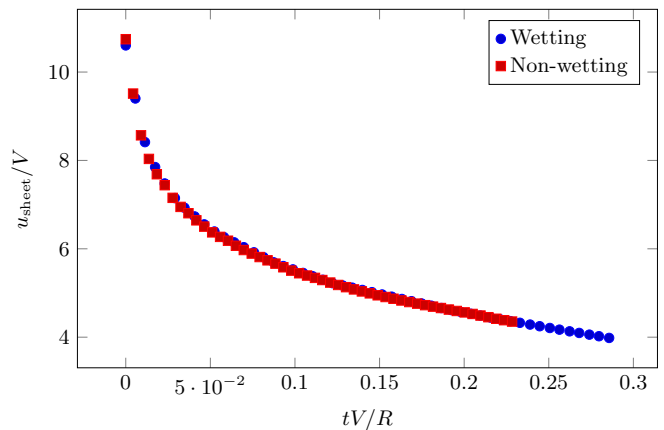


Figure 9. Horizontal liquid sheet ejection velocity as a function of time for a simulated droplet with the parameters of ethanol at atmospheric pressure. Velocities and time are made non-dimensional with the impact velocity V and droplet radius R .

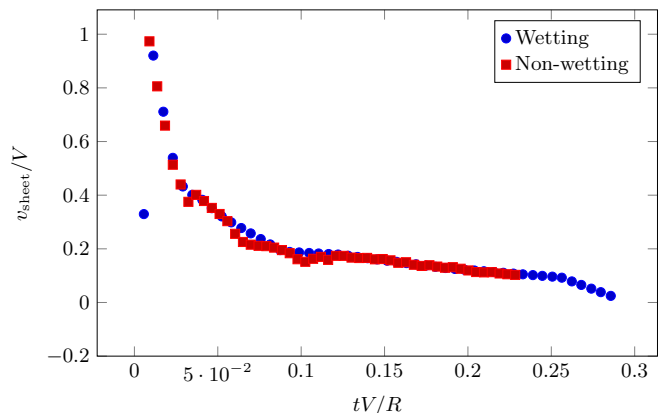


Figure 10. Vertical liquid sheet ejection velocity as a function of time for a simulated droplet with the parameters of ethanol at atmospheric pressure. Velocities and time are made non-dimensional with the impact velocity V and droplet radius R . Wetting and non-wetting surfaces show the same behavior.

moving contact lines. A stationary contact line will approach a homogeneous surface at an angle θ_0 that is determined purely by wetting properties. If the contact line is forced to move, as in the classic case of a solid being plunged into or withdrawn from a liquid bath, the shape of the interface will be determined by both the capillary number, which describes the balance between surface tension and viscous forces, and gravity [1]. In addition, the assumption is made that the contact line is moving slowly enough that the microscopic contact angle is independent of the capillary number and is equal to Young's angle θ_0 , which now serves as a boundary condition at the surface. For advancing contact lines this results in a critical capillary number at which this boundary condition cannot be satisfied [1, 20]. Consequently, theory predicts that above this critical capillary number wetting failure will

be observed in the form of air bubble entrainment at the contact line. Additionally, it is predicted that the critical capillary number depends on the wetting properties of the surface [4].

During drop impact, the motion of the liquid-solid contact line is driven by the inertia of the liquid: the contact line is moving fastest immediately after impact, and proceeds to rapidly decelerate as shown in Fig. 2. Figure 2 further reveals that at the moment of thin sheet formation the capillary number of the contact line is in the unstable regime: at atmospheric pressure $t_{\text{sheet}} = 0.21\text{ms}$ with $\text{Ca}(t_{\text{sheet}}) = 2.9$. Therefore at all times between impact and sheet creation $\text{Ca} > 2.9$.

The time of thin sheet creation varies with multiple parameters, most importantly with the ambient gas pressure. However, in all cases we find that thin sheet creation occurs when $\text{Ca}(t_{\text{sheet}}) \gtrsim 1$. Indeed, for the points shown in Fig. 3 a thin sheet is created with $1.2 < \text{Ca}(t_{\text{sheet}}) < 7.5$, for the 32 cP drops in Fig. 4 $1.6 < \text{Ca}(t_{\text{sheet}}) < 5.1$, and for the 9.4 cP drops in Fig. 4 $0.7 < \text{Ca}(t_{\text{sheet}}) < 3.0$.

The high resolution of our simulations allow us to determine that at such high Ca the contact line is advancing via a "rolling" motion [7]. The resulting $\theta_0 = 180^\circ$ is equivalent to the presence of an ultra-thin air film that extends underneath the drop, as can be seen in Fig. 6(a-c). These results are consistent with Kolinski et al., who found that the leading edge of an impacting drop is not in contact with the surface, but skates over an ultra-thin layer of air [21]. Van der Waals forces between the liquid and substrate rapidly close such an air layer: a 1 nm film would be closed in a fraction of a microsecond [22, 23]. Therefore, although we can identify this air film in simulations that do not include attractive forces between the liquid and solid, we are only able to experimentally detect the thicker gas film that is present after t_{sheet} .

The behavior of the splashing contact line at high Ca provides a means of testing splashing theories, such as the recent work by Riboux and Gordillo [4] or by Liu and Xu [24]. In the Riboux and Gordillo model, the spreading liquid is forced upward by a combination of lubrication and aerodynamic forces. As the liquid edge rises, its rim increases in size due to surface tension and, consequently, the bottom surface of the rim is forced downward. Depending on which of these effects dominates, the lamella either continues moving upward and eventually breaks apart to form a splash, or rewets the substrate, which prevents splashing. The lubrication force calculated is strongly dependent on the shape of the advancing contact line set by the microscopic contact angle. Crucially, this microscopic contact angle is assumed to be indepen-

dent of the contact line velocity. Therefore the authors predict the splashing threshold to strongly depend on the wetting properties of the substrate; this is inconsistent with the results presented here from experiments and simulations. Furthermore, this model predicts that splashing occurs at time $t_{e,\text{crit}}$ after impact, calculated from Eqn. 1 in Ref. [4]. In contrast, we find that in all cases $t_{\text{sheet}} \gg t_{e,\text{crit}}$ [3, 8, 9], often by several orders of magnitude. Together, these results suggest that the microscopic basis of this and similar theories should be revisited. In contrast, Liu and Xu propose that splashing is caused by the Kelvin-Helmholtz instability in the air film that was observed in Ref. [21] and in our simulations. While our results are not a direct test of this model, they are consistent with its implicit θ independence.

IV. CONCLUSION

Splashing arises from the interaction of three phases: the liquid drop, the solid substrate, and the ambient gas. It is therefore surprising that the most basic measure of this interaction, the contact angle θ_0 , does not influence the outcome of drop impact. Our experiments show that both the time of the splash, as well as the splashing thresholds are independent of θ_0 . Direct numerical simulations allow us to probe the advancing liquid-gas interface at nm length scales and show that the shape of this interface is the same for $\theta_0 = 0^\circ$ and $\theta_0 = 180^\circ$.

Splashing occurs when the liquid is spreading rapidly across the substrate, at capillary numbers much greater than unity. In this regime, both experiments [21] and simulations [7] suggest that the advancing contact line spreads over a short-lived thin film of air. Understanding the dynamics of this air film, particularly its rapid growth at t_{sheet} that leads to splashing, as well as how t_{sheet} is set by ambient pressure, is crucial to forming an accurate model of splashing.

ACKNOWLEDGMENTS

This work was supported by the University of Chicago Materials Research and Engineering Center (MRSEC) through grant DMR-1420709 and by the NSF grant DMR-1404841. The VOF simulation method for splashing employed here was developed with support from the Multi-University Research Initiative (MURI) program - Office of Naval Research (MURI) - N00014-11-1-0690.

-
- [1] A. Marchand, T. S. Chan, J. H. Snoeijer, and B. Andreotti, *Physical Review Letters* **108**, 204501 (2012).
 - [2] E. Vandre, M. S. Carvalho, and S. Kumar, *Journal of Fluid Mechanics* **707**, 496 (2012).

- [3] M. M. Driscoll and S. R. Nagel, *Physical Review Letters* **107**, 154502 (2011).
- [4] G. Riboux and J. M. Gordillo, *Physical Review Letters* **113**, 024507 (2014).

- [5] J. H. Snoeijer, B. Andreotti, G. Delon, M. Fermigier, *et al.*, *Journal of Fluid Mechanics* **579**, 63 (2007).
- [6] C. Duez, C. Ybert, C. Clanet, and L. Bocquet, *Nature Physics* **3**, 180 (2007).
- [7] A. M. P. Boelens, A. Latka, and J. J. de Pablo, “Observation of the pressure effect in simulations of droplets splashing on a dry surface,” (2016), arXiv:1601.02134.
- [8] M. M. Driscoll, C. S. Stevens, and S. R. Nagel, *Physical Review E* **82**, 036302 (2010).
- [9] C. S. Stevens, A. Latka, and S. R. Nagel, *Physical Review E* **89**, 063006 (2014).
- [10] L. Xu, W. W. Zhang, and S. R. Nagel, *Physical Review Letters* **94**, 184505 (2005).
- [11] L. Xu, L. Barcos, and S. R. Nagel, *Physical Review E* **76**, 066311 (2007).
- [12] L. Xu, *Physical Review E* **75**, 056316 (2007).
- [13] C. Hirt and B. Nichols, *Journal of Computational Physics* **39**, 201 (1981).
- [14] J. Brackbill, D. Kothe, and C. Zemach, *Journal of Computational Physics* **100**, 335 (1992).
- [15] T. Qian, X.-P. Wang, and P. Sheng, *Physical Review E* **68**, 016306 (2003).
- [16] J.-F. Gerbeau and T. Lelievre, *Computer Methods in Applied Mechanics and Engineering* **198**, 644 (2009).
- [17] OpenCFD Ltd, “OpenFOAM (Version 2.1.0) [Computer software],” (2011).
- [18] A. M. P. Boelens and J. J. de Pablo, “Generalized navier boundary condition for a volume of fluid approach using a finite-volume method,” (2016), arXiv:1604.07880.
- [19] C. S. Stevens, *Europhysics Letters* **106**, 24001 (2014), 1403.3145.
- [20] H. Benkreira and M. Khan, *Chemical Engineering Science* **63**, 448 (2008).
- [21] J. M. Kolinski, S. M. Rubinstein, S. Mandre, M. P. Brenner, D. A. Weitz, and L. Mahadevan, *Physical Review Letters* **108**, 074503 (2012).
- [22] F. B. Wyart and J. Daillant, *Canadian Journal of Physics* **68**, 1084 (1990).
- [23] S. G. Yiantsios and B. G. Higgins, *Journal of Colloid and Interface Science* **147**, 341 (1991).
- [24] Y. Liu, P. Tan, and L. Xu, *Proceedings of the National Academy of Sciences* **112**, 3280 (2015).